Journal of Rare Earths 39 (2021) 67–74

Contents lists available at ScienceDirect

Journal of Rare Earths

journal homepage: http://www.journals.elsevier.com/journal-of-rare-earths

Low-temperature thermocatalytic particulate carbon decomposition via urea solution-combustion derived CeO_2 nanostructures

S.P. Ratnayake [a, b, *], M.M.M.G.P.G. Mantilaka [a, c], C. Sandaruwan [a], D. Dahanayake [a], Y. Pivini Gunasekara [a], S. Jeyasakthy [a], N.M. Gurusinghe [a], U.K. Wanninayake [a], K.M. Nalin de Silva [a, d]

[a] Sri Lanka Institute of Nanotechnology, Nanotechnology and Science Park, Homagama, Sri Lanka
[b] School of Science, Royal Melbourne Institute of Technology University (RMIT), Victoria, 3000, Australia
[c] Postgraduate Institute of Science, University of Peradeniya, Peradeniya, Sri Lanka
[d] Centre for Advanced Materials and Devices (CAMD), Department of Chemistry, University of Colombo, Colombo 00300, Sri Lanka

ARTICLE INFO

Article history:
Received 15 October 2019
Received in revised form
7 February 2020
Accepted 20 February 2020
Available online 27 February 2020

Keywords:
Ceria
Nanoparticles
Soot
Solution combustion
Graphitic carbon nitride
Rare earths

ABSTRACT

A facile, one-pot, urea solution combustion route was utilized to synthesize highly catalytic CeO_2 nanostructures. CeO_2 prepared under varying thermal conditions was characterized by electron microscopy, energy dispersive X-ray spectroscopy, X-ray diffraction, X-ray photoelectron spectroscopy, infrared and Raman techniques. As the synthesis temperature is raised from 400 to 1000 °C, the crystallite size and *d*-spacing of nanoparticles are observed to reduce while cell parameters remain in the same range. Particle size exhibits an accession from ~20 to ~50 nm along the process. Initial CeO_2 nanoparticles are detected as a composite structure of CeO_2 and graphitic carbon nitride (g-C_3N_4) produced by the pyrolysis of urea. Concerning the solid carbon particulate oxidation capacity, an outstanding performance is exhibited by CeO_2 synthesized at 800 °C where the oxidation onset temperature is reduced by 27% compared with the others. The superior performance is attributed to the carbon nitride-generated unique CeO_2 nanomorphology consolidating ample reactive sites and facilitated oxygen delivery for a highly efficient thermocatalytic process. Concerning atmospheric pollution mitigation, synthesis of these CeO_2 nanostructures represents a cost effective and convenient abatement technique for carbon particulates in comparison to cost-intensive, environmentally detrimental and noble-metal based techniques.

1. Introduction

Cerium (Ce) is found principally in rare earth ores such as monazite and bastnaesite around the world concurrently existing with other elements such as zirconium (Zr), lanthanum (La) and thorium (Th).[1] The most stable oxide form of Ce is cerium dioxide (CeO_2) which exists in cubic fluorite phase and renowned for refractory properties alongside elements such as W, V and Zr.[2–6] Oxides of Ce exists in +3 and + 4 oxidation states and it has been reported that Ce_2O_3 with the former oxidation state converts to the latter, upon heating in an oxygen environment forming a structure with Ce at the centre surrounded by eight oxygens in a face cantered cubic orientation.[7–9] CeO_2 is considered to have a high oxygen storage capacity depending on its morphology along with crystal structure and exhibits the ability to conveniently interchange its oxidation state between +3 and +4.[10–12]

CeO_2 nanoparticles (NPs) have attracted significant scientific interest owing to their unique material characteristics and their usability as a heterogeneous catalyst within the liquid and the gas phases is well established.[13–16] CeO_2 is widely adopted in modern-day catalytic converters, automobile exhaust systems, oxygen sensors, solid oxide fuel cells and as a fuel additive facilitating a homogeneous burn.[4,17–21] The intended use of CeO_2 in effluent gas treatment systems is supporting the conversion of compounds such as CO, NO and other hydrocarbons at reactive sites on the Pt–Pd–Rh catalyst by providing ample oxygen.[22,23] Such precious metal-based catalytic systems are efficient, yet the high cost of production hinders their usability in a vast number of potential appliances such as domestic power generators.

* Corresponding author. School of Science, Royal Melbourne Institute of Technology University (RMIT), Victoria, 3000, Australia.
E-mail addresses: s3767930@student.rmit.edu.au, samanthaheyag@gmail.com (S.P. Ratnayake).

https://doi.org/10.1016/j.jre.2020.02.013
1002-0721/

Since morphology and size of CeO_2 NPs are known to critically affect its optical, electronic and catalytic properties, extensive efforts are being made to develop facile methods for size and shape control of NPs.[24] Spherical, rod and dendrite-type morphologies have been reported and sol-gel synthesis remains one of the most popular methods of production.[7,25,26] Other methods include hydrothermal crystallization,[27] flame spray pyrolysis[28] and solvothermal routes.[24,29] In practice, controlling the particle size and morphology during the NP synthesis is known to be challenging due to the vast number of variables governing the crystallization process that are not yet fully understood.[24] Nevertheless, solution combustion synthesis is regarded as considerably advantageous over other methods as it allows a more homogeneous distribution of particle size and morphology while being less labour-intensive.[24,30]

In this study, CeO_2 nanostructures were synthesized utilizing a convenient, urea-assisted, one-pot solution combustion route. Size and morphology of produced NPs were investigated. In addition, compositional, crystallographic and catalytic properties were comparatively investigated in detail for a series of NP batches produced via solution combustion at different temperatures. Elucidations were made on which thermal conditions are suited for producing highly catalytic CeO_2 NPs for the oxidation of solid carbon particulates.

2. Experimental

2.1. Materials

Cerium (lll) acetate (Sigma Adrich-99.99%) was used as the Ce source while granular urea (Central Drug House, New Delhi, India-99.0% assay) was utilized as the combustion fuel source. Nitric acid (Sisco Research Laboratories, Mumbai, India-69%) was used in the dissolution of precursors and all chemicals were utilized as received.

2.2. Synthesis of ceria NPs

0.75 g of cerium acetate was added into 50 mL of 5 mol/L HNO_3 and stirred until complete dissolution. 1.25 g of urea was added into the mixture and was stirred for further 30 min. The resulting solution was placed in a covered ceramic crucible and kept in the muffle furnace (Nabertherm B-180) for 4 h at 400 °C under atmospheric conditions. Three more solutions were prepared and placed at temperatures of 600, 800 and 1000 °C respectively to obtain additional NP batches.

2.3. Characterization

Synthesized CeO_2 NPs were examined under the scanning electron microscope (SEM - Hitachi SU-6600) to investigate the size and morphology. Crystallographic data were obtained via X-ray diffractometry (XRD - Bruker D8 Focus). In addition, Raman/FT-IR spectra (Bruker Vertex 80/Senterra 2) and X-ray photoelectron spectroscopic measurements (XPS – Thermo Escalab 250Xi) were obtained for further information on structure and oxidation states.

2.4. Catalytic oxidation of particulate carbon/soot by synthesized ceria NPs

Prepared CeO_2 NP samples were separately blended with finely ground charcoal particulates in a 1: 4 ratio. The resultant mixtures were subjected to oxidation analysis by placing 20 mg portions from each in the thermogravimeter (TA Instruments, Q-600) and raising the temperature to 1000 °C with a temperature gradient of 20 °C/min.

3. Results and discussion

3.1. Morphological and compositional analysis

The characterization of CeO_2 NPs synthesized by the urea-assisted solution combustion method produced intriguing results in comparison to outcomes reported by peer scientists. Physical appearances, shapes and morphologies of synthesized NPs are depicted in Fig. 1. NPs prepared at 400 °C exhibited an average size of ~20 nm and particles were observed to be aggregated in to spherical structures with a diameter ranging from 100 to 300 nm (Fig. 1(a)). Similar morphologies have been observed for CeO_2 NPs prepared by analogous techniques.[31] An aggregated structure was observed for CeO_2 NPs synthesized at 600 °C as well. The particle size was in the range of 20–40 nm and an aggregate structure with a smoother surface morphology as opposed to the former was observed (Fig. 1(b)). Obtained particle morphologies and sizes were in agreement with reported literature for comparable synthesis and calcination conditions.[32] A distorted spherical morphology with an average particle size in the range of 30–50 nm was observed in NP samples produced at 800 °C in comparison to those obtained at 600 °C (Fig. 1(c)). In terms of particle size, the highest was observed

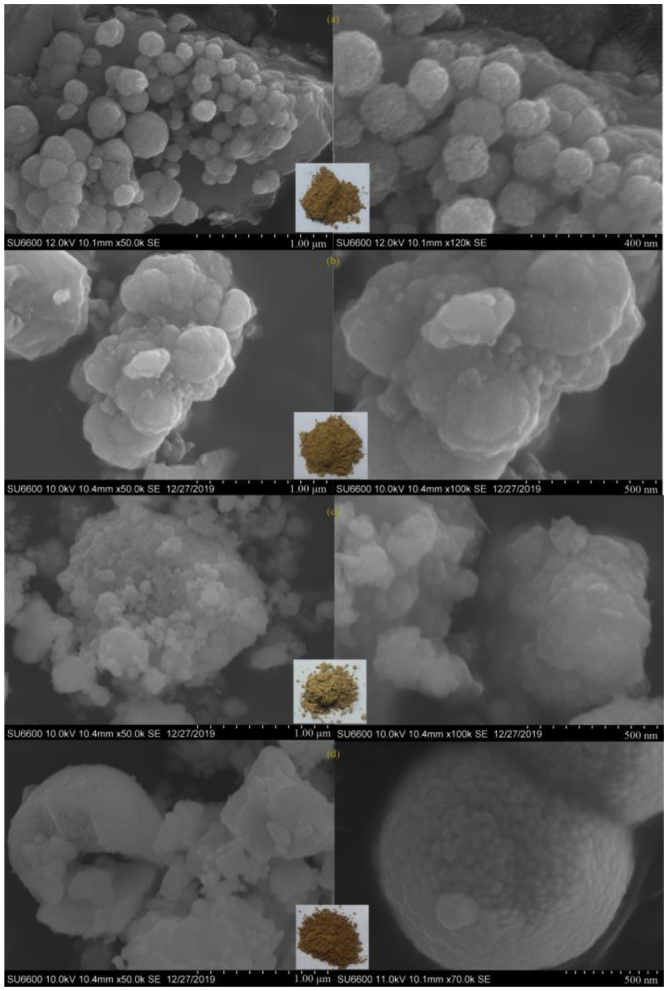

Fig. 1. SEM images and physical appearance of CeO_2 NPs calcined at different temperatures. (a) 400 °C; (b) 600 °C; (c) 800 °C; (d) 1000 °C.

for NPs synthesized at 1000 °C which was in the range of 50 nm (Fig. 1(d)). Highly homogeneous aggregates were detected with an average diameter of ~1 μm which falls in the same range as of those in published comparable studies.[33]

Energy dispersive X-ray (EDX) spectroscopy revealed the basic elemental composition of the samples. Fig. 2 depicts the EDX map images obtained for CeO_2 synthesized at 400 °C. Most prominent elements detected were Ce and O which principally constituted to the bulk of the nanostructures. Carbon and nitrogen signals were simultaneously detected which could be ascribed to g-C_3N_4 present in the sample. Additional impurity elements were not detected implying the absence of inorganic bulk contaminations. Instrumental limitations in quantifying low-molecular-weight elements as well as low abundances hindered quantitative determination of elemental composition. EDX, SEM and transmission electron micrographs (TEM) of pure g-C_3N_4 are provided in supplementary data (S-1).

3.2. Crystallographic analysis

The crystallography of the prepared CeO_2 NP samples was analyzed by XRD and a near-identical peak pattern was obtained for all. Major peaks in the ascending order of intensity were detected at 2θ values of 28.25°, 46.95°, 32.75° and 55.74° (Fig. 3). The dominant peak corresponding to the (111) facet of CeO_2 was detected at 28.25° with the highest intensity for NPs produced at 1000 °C. The cubic fluorite structure of CeO_2 was confirmed while all peak positions were comparable to those of pure ceria found in literature.[33] The (311) facet was almost absent in samples produced below 800 °C and this could have occurred due to the prerequisite of a greater temperature for the formation of NPs with required crystallinity. The increment in synthesis temperature seemed to have caused a more prominent crystallinity at the same time increasing the particle size up to ~50 nm. This occurrence was supported by the presence of narrower XRD peaks and multiple peer research have corroborated the observations.[32,34]

Crystal parameters calculated by the Scherrer's formula based on the strongest peaks are denoted in Table 1. The crystallite size was observed to be smallest in NPs synthesized at 1000 °C whereas;

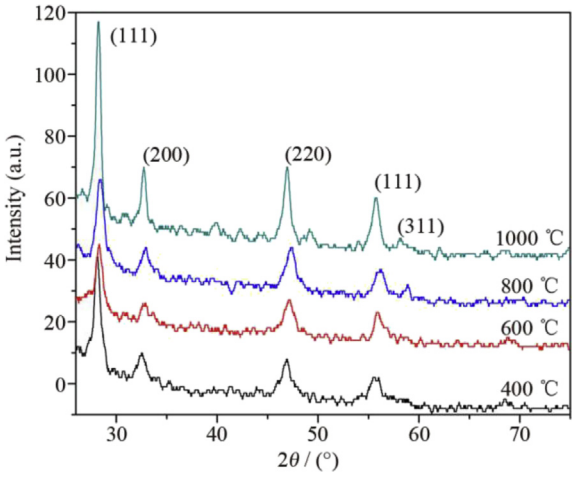

Fig. 3. Comparative XRD spectra of CeO_2 NPs synthesized at different temperatures.

Table 1
Crystallographic parameters of CeO_2 NPs synthesized at different temperatures.

Calcination temperature (°C)	Cell parameters (nm)	*d*-spacing (nm)
400	$a = b = c = 0.54113$ Crystallite size = 32.26	0.3169
600	$a = b = c = 0.54124$ Crystallite size = 35.8	0.3149
800	$a = b = c = 0.54110$ Crystallite size = 27.5	0.3137
1000	$a = b = c = 0.54124$ Crystallite size = 9.81	0.3154

NPs produced at 600 °C exhibited the highest. An increment in unit cell parameters with temperature was identified for samples synthesized at 400 and 600 °C, which was in agreement with published literature as well.[32] Interestingly, the unit cell parameters as well as the *d*-spacing were the lowest in NPs synthesized at 800 °C. A TEM based peer study measuring the *d*-spacing of the (111) facet

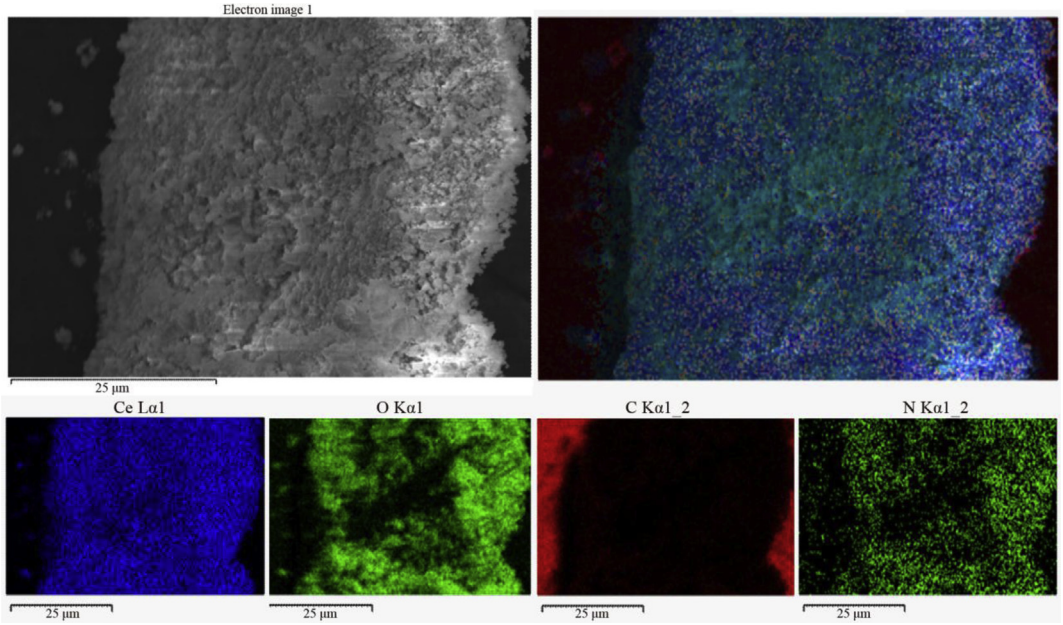

Fig. 2. EDX map images of CeO_2 NPs calcined at 400 °C.

of CeO_2 derived by a comparable method reported values in the same range.[35]

During the standard scan of the sample prepared at 400 °C, a shoulder peak at 27.5° was reluctantly distinguishable which could be attributed to the (002) facet of urea pyrolysis-induced g-C_3N_4 in the initial sample.[35,36] Upon an exhaustive XRD measurement with a significantly enhanced analysis resolution, the two peaks corresponding to (001) and (002) facets of g-C_3N_4 were detected against a fingerprint XRD spectrum of pure g-C_3N_4 (Fig. 4).[36,37]

3.3. Analysis of molecular structure

Prepared NP batches were subjected to an FT-IR analysis to comparatively examine the bond composition (Fig. 5(a)). Spectra components corresponding to CeO_2 of all samples were analogous to those reported in literature.[38,39] The Ce–O stretching vibration was represented as a broad band below 700 cm^{-1} while the broad band at 3430 cm^{-1} was attributed to OH stretching vibrations.[40,41] The peaks characteristic to out-of-plane breathing vibrations of triazine units subsisting within the formed g-C_3N_4 groups were evident in IR spectra at 810 cm^{-1}. In addition, the series of peaks observed within the range of 900–1700 cm^{-1} could be ascribed to stretching modes of C–N heterocyclic (Fig. 5(b)).[35] A strong peak at 1412 cm^{-1} overlapping the above stated range could be attributed to O–O vibrations which were exhibited as most protuberant in the NP sample synthesized at 800 °C.

Raman analysis of synthesized CeO_2 NPs revealed three prominent peak regions of which, one was identified to be caused by overtones (2000–3000 cm^{-1}) of primary peaks (Fig. 6). Among the main peaks, the characteristic F2G mode of CeO_2 representing the cubic fluorite structure belonging to the *Fm*3*m* space group was observed at 449 cm^{-1} which was highest in NPs synthesized at 800 °C. This single active Raman mode is distinctive for a symmetric breathing mode of oxygen atoms as they move around the Ce cation.[34] The same peak was observed to be lowest in the sample synthesized at 600 °C. The broad band observed at ~250 cm^{-1} was attributed to Ce–O bonds while the sharp peak present at ~580 cm^{-1} was imparted by the available oxygen vacancies formed during the thermal treatment of the CeO_2 matrix.[34,42,43] Availability of surface oxygen vacancies could also be a sign of a defect-rich structure which could have resulted in substantial reactive sites on the surface. As discussed earlier, the symmetric breathing mode of O atoms around each cation is the strongest in CeO_2 synthesized at 800 °C, thus making it a well-suited temperature to synthesize catalytically efficient CeO_2.

An XPS analysis was carried out to investigate the chemical composition and available elemental oxidation states in NPs (Fig. 7). Ce, C, N and O were detected as principal elements with O

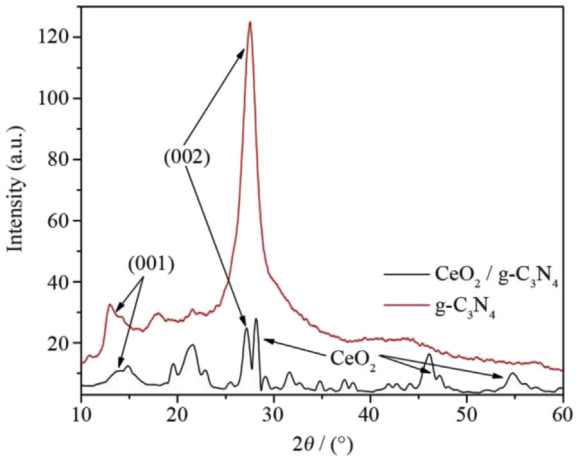

Fig. 4. Comparative XRD spectra of pure g-C_3N_4 and CeO_2 prepared at 400 °C.

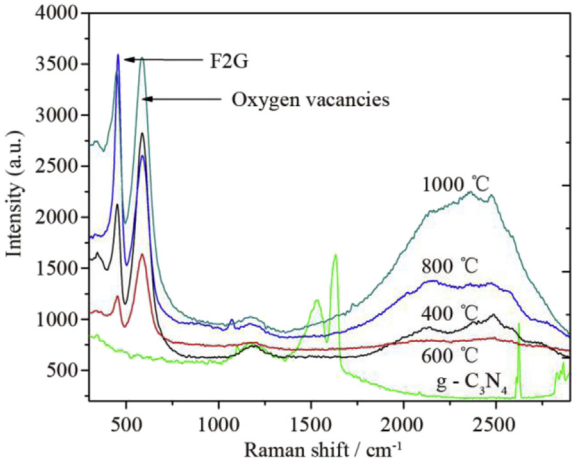

Fig. 6. Raman spectra of CeO_2 NPs synthesized at different temperatures.

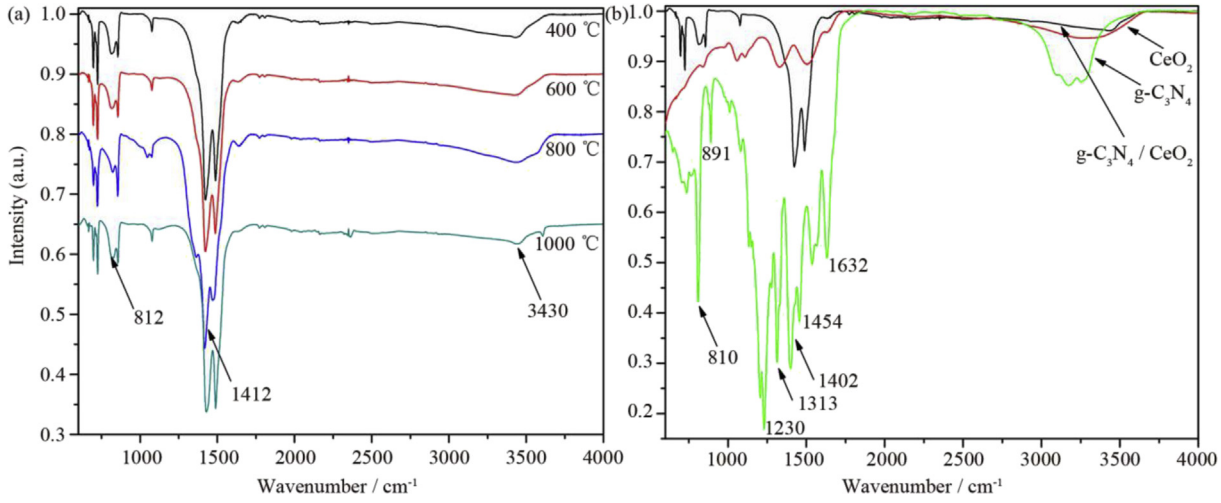

Fig. 5. Comparative FT-IR spectra of CeO_2 NPs synthesized at different temperatures (a) and comparative spectra of pure g-C_3N_4 and CeO_2 (b).

exhibiting the highest abundance (Fig. 7, Supplementary data: S-2 and S-T 1). This may have been a complimentary effect of O in the binary oxide as well as O bound to the surface. In NPs synthesized at 400 °C, Ce was readily detected in a single oxidation state as Ce^{4+}. Peaks with binding energies (BEs) 883.3, 889.7 and 897.6 eV (Fig. 7(a)) were attributed to $3d_{5/2}$ spin state of Ce^{4+} while peaks at 903, 907.4 and 916.7 eV (Fig. 7(a)) were ascribed to $3d_{3/2}$ spin state of Ce^{4+}. Samples prepared at 400 and 800 °C exhibited analogous peaks structures (Fig. 7(a, b)). Oxygen was indicated mainly in two chemical environments having respective BEs as 528.9 and 531.7 eV. With respect to published data, these peaks in the given order could be ascribed as O present in CeO_2 matrix covalently bound to Ce and O vacancies on the surface. In addition, a weak peak in sample prepared at 800 °C corresponding to surface bound O in the form of adventitious OH groups was observed at 534.9 eV[44–46] (Fig. 7(c, d)). Spectra of the sample synthesized at 400 °C exhibited three major peaks at respectively 284.8 eV representing C–C chemical environment, 286.4 eV corresponding to C_3N environment and 293.4 eV signifying two coordinated C atoms in the nanostructure[47,48] (Fig. 7(e)). Adventitious C may have also contributed sparingly to the C content in samples. N spectrum of NPs synthesized at 400 °C exhibited a single peak at 399.8 eV which corresponds to a three coordinated N atomic environment (N_{3C}) while the samples prepared at higher temperatures indicated additional peaks.[47] NPs prepared at 800 °C revealed peaks respectively at 397.8, 403.5 and 407.2 eV which were ascribed to Ce–N, N–N and NO_3^- environments (Fig. 7(f)).[40,47,48] In this case, the increase in the synthesis temperature to 800 °C may have intensified precursor interactions hence facilitating nucleation and growth of composite NPs with favorable thermocatalytic attributes. The highest O content was detected in NPs synthesized at 800 °C, implying the high favorability and potential for facilitating catalytic oxidation. Obtained XPS results seemed to compliment FT-IR and Raman based data substantiating an active-site rich catalyst

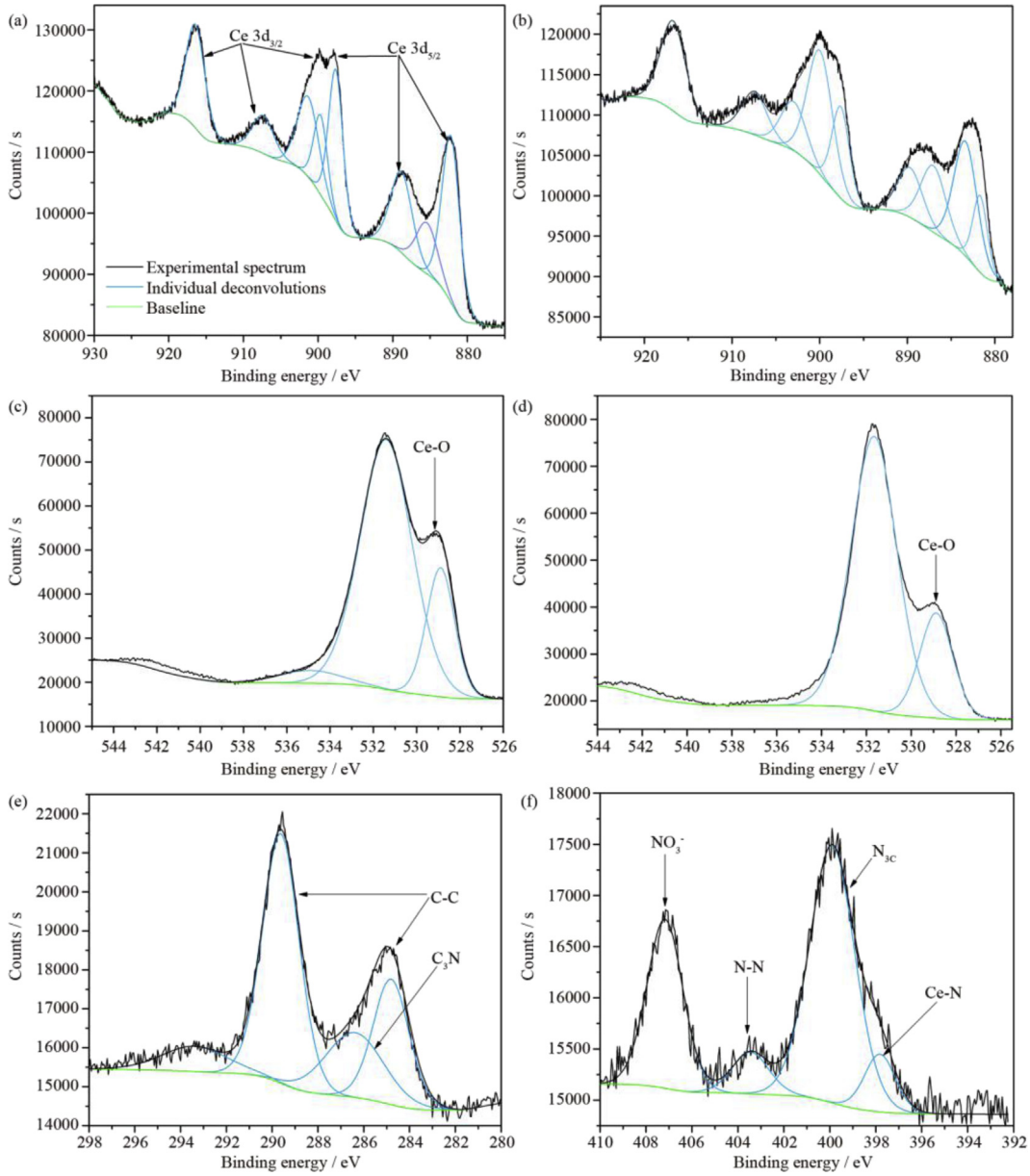

Fig. 7. XPS spectra for derived CeO_2 samples - Narrow scan spectra for samples derived at: Ce - 800 °C (a) and 400 °C (b), oxygen - 800 °C (c) and 400 °C (d), carbon - 800 °C (e) and nitrogen - 800 °C (f). Legend in Fig. 7(a) applies to all plots.

surface. XRD based observations corroborated the XPS outputs implying the initial formation of a CeO_2/g-C_3N_4 combined nanostructure via the urea assisted solution combustion of the precursor mixture.[49]

3.4. Thermal characterization

In order to quantify the carbonaceous content in the prepared nanomaterial, the sample was subjected to a TGA analysis (Fig. 8). A prominent weight loss corresponding to a percentage of 4.23% was observed upon heating the sample with a temperature gradient of 20 °C/min and it was attributed to the decomposition of the g-C_3N_4 component.

Thermocatalytic activity on oxidation of carbon particulates was evaluated by preparation of a mixture of pure, fine charcoal particles with synthesized NPs and subjecting it to a thermal treatment under atmospheric conditions. It was observed that pure charcoal began oxidizing at ~550 °C while all samples in contact with CeO_2 NPs exhibited an earlier oxidation onset point (Fig. 9). CeO_2 NPs synthesized at 400, 600 and 1000 °C behaved in a similar manner, indicating an oxidation onset point for charcoal at ~500 °C. Interestingly, NPs synthesized at 800 °C showed a distinctively early oxidation onset point around 400 °C.

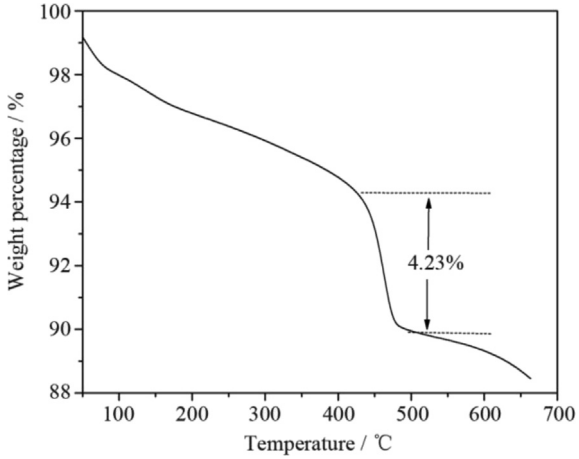

Fig. 8. TGA analysis of CeO_2/g-C_3N_4 sample.

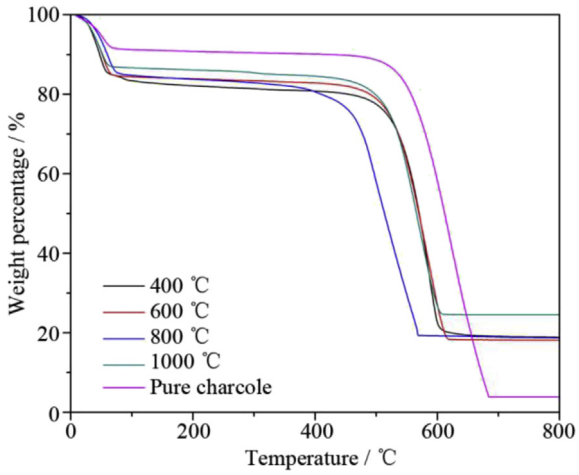

Fig. 9. Oxidation capability of carbon by CeO_2 NPs synthesized at varying temperatures.

Previous observations indicated the presence of a g-C_3N_4 incorporated CeO_2 matrix in the primary NPs, thus the complimentary behavior of the two seemed to transfigure superior thermocatalytic attributes in the composite during the thermal treatment process. The optimal availability of reactive sites and oxygen deliverability for the catalytic process influenced through favorable particle size, morphology and the crystal defect structure of NPs could have led to the outstanding performance of the CeO_2 synthesized at 800 °C.

Based on numerous studies, it has been substantiated that CeO_2 is efficient as a standalone or combined heterogeneous catalyst.[50,51] g-C_3N_4 is a polymeric semiconductor material with a commendable thermal and chemical stability. It is renowned for its defect-rich, nitrogen bridged poly(tri-s-triazine) shell and use of it as a photocatalyst has been widely practiced owing to its narrow band structure.[35,40] Numerous researchers have achieved synthesis of g-C_3N_4 via a simple pyrolytic reaction involving urea.[36,37] The formation takes place around 500 °C in an enclosed reaction chamber where urea converts to $C_3N_6H_6$ before transforming to g-C_3N_4. The precursor has been shown to evaporate before reaching 400 °C unless the reaction environment is enclosed. Furthermore, formed g-C_3N_4 is known to be completely thermally decomposed above 600 °C.[37]

A recent study has provided new insights into the heightened catalytic activities of metal oxide nanoparticles derived via combustion assisted methods utilizing C and N containing precursor compounds.[49] It has been established that during the initial stage of the combustion where the temperatures are below 550 °C, the C and N based fuel (e.g. dicyanamide/urea) vigorously undergoes conversion to g-C_3N_4 which subsequently encapsulates the nucleating metal oxide nanoparticles. With time the C/N based fuel becomes completely consumed by the reaction. As the temperature elevates above 600 °C, the formed g-C_3N_4 begins to decompose exposing the metal oxide (CeO_2) surface and the decomposition directs extensive formation of lattice features such as surface defects, edge defects and active sites on the substrate surface. These features eventually becomes crucial in the catalytic performance of the final nanostructures.[49] Surface features such as oxygen vacancies can arise due to stated circumstances and their presence was pronounced in Raman and XPS outputs. During the urea-assisted solution combustion, the unique environment created by the enclosed and confined combustion chamber is believed to contribute positively to the formation of the nanostructures as well.[36,49] The solution combustion process is known to provide a controlled release of the constituents during the reaction phase facilitating a greater interaction among reactant species, hence driving the reaction forward successfully.[36] The covered crucible becomes instrumental in containment of the Ce^{3+}/urea solution medium and the initially formed gaseous cyanic acid for a prolonged duration so that the CeO_2 incorporated polymerized g-C_3N_4 species can be formed.

When utilized for catalytic abatement of particulate carbon, the nanoparticles showed promise by reducing the usual oxidation temperature by a maximum of 27%. We hypothesize the mechanism of this catalytic oxidation reaction to take place through a series of complimentary processes. During the initial step, adsorption of oxygen molecules on ample reactive sites on the surface of the CeO_2 substrate is taken place. Due to the newly formed O_2—CeO_2 bond, molecular O—O bond weakens allowing C in the particulate to react with O and evolve as CO which is subsequently converted to CO_2 via further reaction with O_2 at the CeO_2 surface. Simultaneously, Ce^{4+} reduces to Ce^{3+} accommodating formed O in to the lattice which is then transported through the lattice by alternative interconversion between Ce^{4+} and Ce^{3+}. This process actively transports O to C sites throughout the lattice

where C can be readily oxidized giving rise to a rapid overall particulate carbon abatement process. The NPs synthesized at 800 °C seems to best facilitate this process due to its higher availability of active sites and O vacancies. A notable observation of this study was the reduced cell parameters and the *d*-spacing of CeO_2 NPs synthesized at 800 °C. Reduced cell dimensions are an indication of a smaller unit cell and a decreased *d*-spacing signifies a more compact packing within the matrix. Other than mechanisms stated above, this factor may have contributed in a more efficient oxygen transport process through the matrix resulting in rapid oxidation of carbon particulates at a lower temperature.

CeO_2 is a promising catalyst in widespread use due to its effectiveness in conjunction with added advantages such as inertness and biocompatibility. The currently utilized Pt/Pd/Au system for gaseous and liquid phase conversions is efficient yet is unfavorable from an economic perspective.[52] The outstanding capability exhibited by CeO_2 makes it a formidable candidate for a number of advanced catalytic applications, specifically in automobile exhaust systems, where particulate carbon may be incorporated with hazardous aromatic compounds such as benzo-a-pyrene and other 5/6 ringed polycyclic aromatic compounds.[53] A thermocatalytic system which could readily oxidize carbonaceous compounds altogether may be invaluable regarding mitigation of atmospheric pollution.

4. Conclusions

Solution combustion method was recognized to be a promising approach in synthesis of CeO_2 nanostructures with varying particle size and morphology. Particle size was observed to increase with calcination temperature and the smallest particle diameter was around 20 nm while the highest was in the range of 50 nm. XRD and FT-IR patterns exhibited comparative results to those reported in literature while Raman and XPS spectra indicated an increasing extent of oxygen vacancies as the synthesis temperature was elevated to 800 °C. A commendable carbon particulate oxidation capability was exhibited by CeO_2 NPs synthesized at 800 °C at a significantly reduced temperature. The enhancement could be attributed to the initial formation of g-C_3N_4 which mediates as a template for the generation of defect-rich reactive sites on the CeO_2 surface and its optimal volume of oxygen vacancies. In addition, a denser packing in the CeO_2 matrix favoring a more efficient oxygen transport within the nanomaterial could have contributed in the process. With further tuning, the synthesized nanostructures could become a cost efficient, environmentally friendly catalyst for commercial particulate carbon abatement.

Acknowledgement

Research activities stated in this article were conducted utilizing resources of Sri Lanka Institute of nanotechnology (SLINTEC). Authors wish to acknowledge the invaluable support provided by Dr. Gayan Priyadharshana for conducting and analysis of XPS measurements. Furthermore, we extend our thanks to the staff members of Sri Lanka Institute of Nanotechnology (SLINTEC) for their kind support.

Appendix A. Supplementary data

Supplementary data to this article can be found online at https://doi.org/10.1016/j.jre.2020.02.013.

References

1. Dahle JT, Arai Y. Environmental geochemistry of cerium: applications and toxicology of cerium oxide nanoparticles. *Int J Environ Res*. 2015;12(2):1253.
2. Senkov ON, Miracle DB, Chaput KJ, Couzinie JP. Development and exploration of refractory high entropy alloys—a review. *J Mater Res*. 2018;33(19):3092.
3. Ratnayake S, De Silva N, Kaupuge T, Weerasekera T, Yapa MS, Karunaratne V, et al. Oxidation protection of carbon fiber by sol-gel derived boron doped yttria stabilized zirconia coatings. *Mat Sci Eng B-Adv*. 2018;229:59.
4. Ratnayake S, Mantilaka M, Sandaruwan C, Dahanayake D, Murugan E, Kumar S, et al. Carbon quantum dots-decorated nano-zirconia: a highly efficient photocatalyst. *Appl Catal, A*. 2019;570:23.
5. Goh KL, Thomas S, De Silva RT, Aswathi M. *Interfaces in particle and fibre reinforced composites: current perspectives on polymer, ceramic, metal and extracellular matrices*. 1st ed. Woodhead Publishing; 2019.
6. Ratnayake SP. Characterization studies of ceramic-based composites related to functionalized filler-matrix interface. In: Goh KL, Thomas S, De Silva RT, Aswathi M, eds. *Interfaces in particle and fibre reinforced composites: current perspectives on polymer, ceramic, metal and extracellular matrices*. Amsterdam: Elsevier; 2020:369.
7. Mortensen A. *Concise encyclopedia of composite materials*. 2nd ed. Elsevier; 2006.
8. Preisler E, Marsh O, Beach R, McGill T. Stability of cerium oxide on silicon studied by X-ray photoelectron spectroscopy. *J Vac Sci Technol B*. 2001;19(4):1611.
9. Nadjia L, Abdelkader E, Naceur B, Ahmed B. CeO_2 nanoscale particles: synthesis, characterization and photocatalytic activity under UVA light irradiation. *J Rare Earths*. 2018;36(6):575.
10. Nakagawa K, Tezuka Y, Ohshima T, Katayama M, Ogata T, Sotowa, et al. Formation of cerium carbonate hydroxide and cerium oxide nanostructures by self-assembly of nanoparticles using surfactant template and their catalytic oxidation. *Adv Powder Technol*. 2016;27(5):2128.
11. Si R, Flytzani-Stephanopoulos M. Shape and crystal-plane effects of nanoscale ceria on the activity of Au-CeO_2 catalysts for the water–gas shift reaction. *Angew Chem*. 2008;120(15):2926.
12. Zhang YH, Cui MS, Hou YK, Huang XW, Zhang YQ, Xue QN. Effect of grain size on thermal stability and oxygen storage capacity of $Ce_{0.17}Zr_{0.73}La_{0.02}Nd_{0.04}Y_{0.04}O_2$ solid solutions. *J Rare Earths*. 2019;37(2):178.
13. Liao X, Zhang Y, Hill M, Xia X, Zhao YX, Jiang Z. Highly efficient Ni/CeO_2 catalyst for the liquid phase hydrogenation of maleic anhydride. *Appl Catal A-Gen*. 2014;488:256.
14. Macedo AG, Fernandes SE, Valente AA, Ferreira RA, Carlos LD, Rocha J. Catalytic performance of ceria nanorods in liquid-phase oxidations of hydrocarbons with tert-butyl hydroperoxide. *Molecules*. 2010;15(2):747.
15. Bera P, Aruna S, Patil K, Hegde M. Studies on Cu/CeO_2: a new NO reduction catalyst. *J Catal*. 1999;186(1):36.
16. Zhu T, Flytzani-Stephanopoulos M. Catalytic partial oxidation of methane to synthesis gas over Ni–CeO_2. *Appl Catal*. 2001;208(1–2):403.
17. Korsvik C, Patil S, Seal S, Self WT. Superoxide dismutase mimetic properties exhibited by vacancy engineered ceria nanoparticles. *Chem Commun*. 2007;(10):1056.
18. Boaro M, Vicario M, de Leitenburg C, Dolcetti G, Trovarelli A. The use of temperature-programmed and dynamic/transient methods in catalysis: characterization of ceria-based, model three-way catalysts. *Catal Today*. 2003;77(4):407.
19. Muroyama H, Hano S, Matsui T, Eguchi K. Catalytic soot combustion over CeO_2-based oxides. *Catal Today*. 2010;153(3):133.
20. Shimokawa H, Kurihara Y, Kusaba H, Einaga H, Teraoka Y. Comparison of catalytic performance of Ag-and K-based catalysts for diesel soot combustion. *Catal Today*. 2012;185(1):99.
21. Tana, Zhang ML, Li J, Li HJ, Li Y, Shen WJ. Morphology-dependent redox and catalytic properties of CeO_2 nanostructures: nanowires, nanorods and nanoparticles. *Catal Today*. 2009;148(1):179.
22. Zimmermann S, Messerschmidt J, von Bohlen A, Sures B. Uptake and bioaccumulation of platinum group metals (Pd, Pt, Rh) from automobile catalytic converter materials by the zebra mussel (Dreissena polymorpha). *Environ Res*. 2005;98(2):203.
23. Fornasiero P, Balducci G, Kaspar J, Meriani S, di Monte R, Graziani M. Metal-loaded CeO_2-ZrO_2 solid solutions as innovative catalysts for automotive catalytic converters. *Catal Today*. 1996;29(1–4):47.
24. Fu C, Li RX, Zhang Y. Synthesis and crystallization of nano-ceria particles by solvothermal routes. *Int J Mod Phys B*. 2010;24(15n16):3230.
25. Gnanam S, Rajendran V. Synthesis of CeO_2 or α–Mn_2O_3 nanoparticles via sol-gel process and their optical properties. *J Sol-Gel Sci Techn*. 2011;58(1):62.
26. Xiao H, Ai Z, Zhang L. Nonaqueous sol–gel synthesized hierarchical CeO_2 nanocrystal microspheres as novel adsorbents for wastewater treatment. *J Phys Chem C*. 2009;113(38):16625.
27. Tok A, Du S, Boey F, Chong W. Hydrothermal synthesis and characterization of rare earth doped ceria nanoparticles. *Mater Sci Eng*. 2007;466(1):223.
28. Mädler L, Stark W, Pratsinis S. Flame-made ceria nanoparticles. *J Mater Res*. 2002;17(06):1356.
29. Zawadzki M. Preparation and characterization of ceria nanoparticles by microwave-assisted solvothermal process. *J Alloys Compd*. 2008;454(1):347.

30. Masui T, Hirai H, Imanaka N, Adachi G, Sakata T, Mori H. Synthesis of cerium oxide nanoparticles by hydrothermal crystallization with citric acid. *J Mater Sci Lett*. 2002;21(6):489.
31. Zhang DS, Qian YL, Shi LY, Mai HL, Gao RH, Zhang JP, et al. Cu-doped CeO_2 spheres: synthesis, characterization, and catalytic activity. *Catal Commun*. 2012;26:164.
32. Maensiri S, Masingboon C, Laokul P, Jareonboon W, Promarak V, Anderson PL, et al. Egg white synthesis and photoluminescence of platelike clusters of CeO2 nanoparticles. *Cryst Growth Des*. 2007;7(5):950.
33. Khakpour Z, Yuzbashi A, Maghsodipour A, Ahmadi K. Electrical conductivity of Sm-doped CeO_2 electrolyte produced by two-step sintering. *Solid State Ionics*. 2012;227:80.
34. Deus R, Cortés J, Ramirez M, Ponce MA, Andres J, Rocha L, et al. Photoluminescence properties of cerium oxide nanoparticles as a function of lanthanum content. *Mater Res Bull*. 2015;70:416.
35. Tian N, Huang HM, Liu CY, Dong F, Zhang TR, Du X, et al. *In situ* co-pyrolysis fabrication of CeO_2/gC_3N_4 n–n type heterojunction for synchronously promoting photo-induced oxidation and reduction properties. *J Mater Chem*. 2015;3(33):17120.
36. Liu JH, Zhang TK, Wang ZC, Dawson G, Chen W. Simple pyrolysis of urea into graphitic carbon nitride with recyclable adsorption and photocatalytic activity. *J Mater Chem*. 2011;21(38):14398.
37. Chidhambaram N, Ravichandran K. Single step transformation of urea into metal-free g-C_3N_4 nanoflakes for visible light photocatalytic applications. *Mater Lett*. 2017;207:44.
38. Kumar S, Ojha AK. Ni, Co and Ni–Co codoping induced modification in shape, optical band gap and enhanced photocatalytic activity of CeO_2 nanostructures for photodegradation of methylene blue dye under visible light irradiation. *RSC Adv*. 2016;6(11):8651.
39. Zamiri R, Ahangar HA, Kaushal A, Zakaria A, Zamiri G, Tobaldi D, et al. Dielectrical properties of CeO_2 Nanoparticles at different temperatures. *PloS One*. 2015;10(4):e0122989.
40. Tan LH, Xu JH, Zhang XJ, Hang ZS, Jia YQ, Wang SB. Synthesis of g-C_3N_4/CeO_2 nanocomposites with improved catalytic activity on the thermal decomposition of ammonium perchlorate. *Appl Surf Sci*. 2015;356:447.
41. Periyat P, Laffir F, Tofail S, Magner E. A facile aqueous sol–gel method for high surface area nanocrystalline CeO_2. *RSC Adv*. 2011;1(9):1794.
42. Reddy BM, Thrimurthulu G, Katta L, Yamada Y, Park SE. Structural characteristics and catalytic activity of nanocrystalline ceria–praseodymia solid solutions. *J Phys Chem C*. 2009;113(36):15882.
43. Liang F, Yu Y, Zhou W, Xu X, Zhu Z. Highly defective CeO_2 as a promoter for efficient and stable water oxidation. *J Mater Chem*. 2015;3(2):634.
44. Gruzalski G, Zehner D, Wendelken J. An XPS study of oxygen adsorption on Cu (110). *Surf Sci*. 1985;159(2–3):353.
45. Brundle C. Oxygen adsorption and thin oxide formation at iron surfaces: an XPS/UPS study. *Surf Sci*. 1977;66(2):581.
46. Sreekanth TVM, Nagajyothi PC, Reddy GR, Shim J, Yoo K. Urea assisted ceria nanocubes for efficient removal of malachite green organic dye from aqueous system. *Sci Rep*. 2019;9(1):1.
47. Kesarla MK, Fuentez-Torres MO, Alcudia-Ramos MA, Ortiz-Chi F, Espinosa-González CG, Aleman M, et al. Synthesis of g-C_3N_4/N-doped CeO_2 composite for photocatalytic degradation of an herbicide. *J Mater Res Technol*. 2019;8(2):1628.
48. Gao D, Liu Y, Liu P, Si M, Xue D. Atomically thin B doped g-C_3N_4 nanosheets: high-temperature ferromagnetism and calculated half-metallicity. *Sci Rep*. 2016;6:35768.
49. Eissa AA, Peera SG, Kim NH, Lee JH. g-C_3N_4 templated synthesis of Fe_3C@NSC electrocatalyst enriched with Fe-N_x active sites for efficient oxygen reduction reaction. *J Mater Chem*. 2019;7(28):16920.
50. Montini T, Melchionna M, Monai M, Fornasiero P. Fundamentals and catalytic applications of CeO_2-based materials. *Chem Rev*. 2016;116(10):5987.
51. Wang S, Lu GM. Role of CeO_2 in Ni/CeO_2–Al_2O_3 catalysts for carbon dioxide reforming of methane. *Appl Catal, B*. 1998;19(3–4):267.
52. Wei YC, Zhao Z, Jiao JQ, Liu J, Duan AJ, JIANG GY. Preparation of ultrafine Ce-based oxide nanoparticles and their catalytic performances for diesel soot combustion. *J Rare Earths*. 2014;32(2):124.
53. Ratnayake SP, Wingfors H. Determination of airborne PAHs using passive sampling with 2, 6 diphenyl-p-phenylenoxide as adsorbant. *J Natl Sci Found*. 2017;45(1):83.